Journal of Membrane Science & Research

journal homepage: www.msrjournal.com

Research Paper

The Real Seawater Pre-Treatment Performance of Trimesic Acid-Based Nanofiltration Membranes Impregnated with Ethylenediamine-MWCNT

Rajesha Kumar Alambi *, Mansour Ahmed , Garudachari Bhadrachari , Mansour Al- Rughaib , Jibu Pallickel Thomas

Water Research Center, Kuwait Institute for Scientific Research, P.O. Box, 24885, 13109 Safat, Kuwait

Article info

Received 2022-10-13
Revised 2022-12-25
Accepted 2023-01-08
Available online 2023-01-08

Keywords

Modified nanoparticles
Seawater pre-treatment
Polymer composite
Desalination
Salt rejection
Flux

Highlights

- A facile approach for the synthesis of a novel phosphonic acid derivative of TiO_2 ($PTiO_2$) nanoparticles is presented.
- The $PTiO_2$ showed high dispersion during the synthesis of thin film nanocomposite (TFN) membranes.
- The boron adsorption by $PTiO_2$ followed a pseudo-second-order kinetics indicating a chemisorption process.
- The TFN membranes showed low boron diffusion at neutral and basic pH due to adsorption and electrostatic repulsive interaction

Graphical abstract

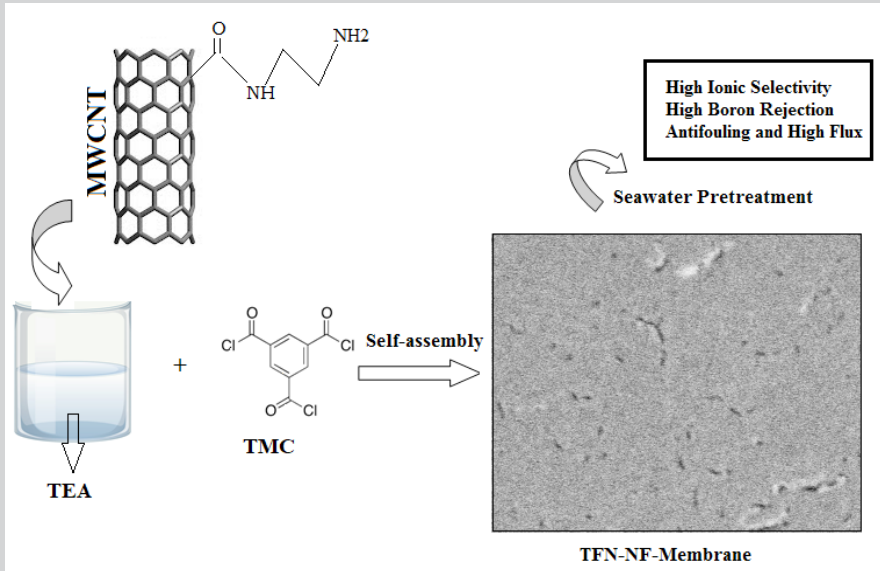

Abstract

Seawater desalination is becoming vital as a means of securing a strategic and sustainable source of water around the world. Membrane-based nanofiltration (NF) is a potential choice for seawater pre-treatment in desalination plants to improve water recovery and plant reliability. The aim of this study is the synthesis of ethylenediamine-modified multiwalled carbon nanotube (EDA-MWCNT) incorporated thin film nanocomposite membranes using a molecular self-assembly approach over the ultrafiltration membrane support. The newly developed membranes were tested for their potential application in Persian Gulf seawater pretreatment using a custom-made pilot scale NF test unit. This study also includes a detailed characterization of the synthesized membranes, evaluation of their boron rejection, and antifouling characteristics. The NF corresponding to the optimal loading of EDA-MWCNT at 0.05wt% (M3) was highly negatively charged, and hydrophilic, and attained denser structures on their surface to attain the flux in the range of 12.0 to 14.0 $Lm^{-2}h.^{-1}$ The total dissolved solids (TDS) of the permeate declined to the lowest value of 9,635 ppm from the initial seawater TDS of 34,560 ppm. Interestingly, the rejection offered by the M3 membrane towards the monovalent ions and boron was higher than the control and other commercial NF membranes. Therefore, EDA-MWCNT as a nanofiller demonstrated its high efficiency to reduce seawater salinity to apply the membrane for water softening applications with higher efficiency than the commercial NF-90, TS-80 4040, and NF-270 membranes.

1. Introduction

Desalination through membrane-based reverse osmosis (RO) is becoming vital as a means of securing a strategic and sustainable source of water around the world. RO technology is also leading the international market for potable and domestic water production in terms of high-water recovery compared to thermal desalination technologies. Advanced RO technology has several benefits to overcome the challenges faced by thermal desalination technologies. Any desalination process must be reliable and robust as well as have low operational expenditure for its long-term sustainability [1]. Currently, most of the GCC countries have implemented SWRO desalination technologies specifically to augment water recovery, facilitate the operation of the

* Corresponding author: rajeshakumar15@yahoo.com (R. K. Alambi)

DOI: 10.22079/JMSR.2023.563446.1570

desalination plants, consume less energy, and achieve the high quality of water achieved by the RO technologies [2]. However, the stringent seawater chemistry of the Persian Gulf's seawater limits RO water recovery compared to other parts of the world [3]. Furthermore, RO suffers from severe membrane fouling due to high pressure, and this has a negative impact on the long-term performance of RO membranes [4]. Thus, the primary challenge for the desalination industry is to produce fresh water with minimal energy and cost. Therefore, such limitations can be addressed by adopting proper and efficient seawater pretreatment technology before feeding the seawater into the RO units.

A proper seawater pretreatment approach is highly desired to maintain the consistent performance and life span of any desalination process. Proper selection of pretreatment methods for feed water will prevent or minimize deterioration in freshwater production; fouling and scaling limitations; corrosion problems; chemical additives; frequent chemical cleanings; ecological problems; and operational costs. Pre-treatment processes for seawater RO are either conventional (for example, dissolved air flotation (DAF) or clarification followed by media filtration) or make use of membrane technologies. Conventional forms of pre-treatment take up much space, and are prone to operational upsets, while polymeric membrane-based nanofiltration (NF) pretreatment technologies are more prominent.

NF as a pretreatment may find a solution for current water recovery issues in multi-stage flash (MSF) (~10%) and RO (~35%). The removal of sulfate, magnesium, and calcium using the NF technology will reduce the scaling and fouling issues in MSF and RO processes to increase water recovery. Until now, commercially available TFC-NF membranes have been investigated for pretreatment application. However, fouling is the major issue with TFC membranes, resulting in reduced NF membrane life and a poor-quality feed water stream for the RO process.

Recently, there are several laboratory-scale membrane development efforts to address the issues faced by NF membranes. Dong et al. synthesized hollow fiber NF membrane by layer-by-layer assembly of polymers for seawater pretreatment application [5]. The resultant NF membrane showed high divalent ionic rejection towards Mg^{2+}, Ca^{2+}, and Sr^{2+} which was attributed to the cationic amine groups on the membrane surface. However, the same amine groups showed lower rejection towards SO_4^{2-} and Cl^- due to the dominating effect of adsorption compared to the size exclusion or Donnan effect. Zhang et al. created a new NF membrane by combining 2,2′-benzidinedisulfonic acid (in the aqueous phase) and trimesoyl chloride reagent (in the organic phase) [6]. The resulting membranes were highly negatively charged and showed high rejection toward Ca^{2+} and SO_4^{2-} ions. The resultant membrane showed high resistance to the gypsum scaling commonly encountered during seawater desalination in the RO process. The gypsum anti-scaling results shown by the newly synthesized membrane were much higher than the commercial NF270 membrane. Alhweij et al. synthesized sulfonated polyaniline NF membranes for the removal of natural organic matter (NOM) from seawater [7]. The NOM removal efficiency of the synthesized NF membranes was higher than the commercial NF membrane and the other conventional pretreatment approaches adopted in the seawater pretreatment. Also, the new membrane witnessed a slightly higher removal of chemical oxygen demand (COD) (74%), compared to the commercial membrane (70%) and conventional treatment (70%). The fouling study revealed a higher flux recovery value for the sulfonated polyaniline NF membrane tested for the sample containing high NOM. Mousavi and Kargari evaluated the efficiency of three different commercial TW30, NE70, and NE90 membranes in the treatment of RO brine [8]. The membrane flux and rejection increased with the increased hydraulic pressure and flow rate of the feed. The TW30 membrane witnessed the highest Total Dissolved Solids (TDS) removal of up to 93% with a permeability of $2.84 Lm^{-2}h^{-1}bar.^{-1}$ The same membrane showed the highest rejection of 98.7, 96.1, and 90.3% towards Mg^{2+}, Ca^{2+}, and Cl^{-1} ions, respectively. The NE70 membrane showed the highest permeability with the least rejection of the ions. Zhang et al. used a modified protocol to synthesize the NF membrane comprised of piperazine and trimesoyl chloride [9]. During the interfacial reaction, phytic acid dodecasodium salt was used as an additive along with the aqueous amine monomer to lower the diffusion of an amine into the acid chloride. The resultant polyamide membrane was thin, in the range of 50 nm, resulting in two times higher flux than the nascent membrane without scarifying the salt rejection. Yang et al. adopted a new technique of metal-organophosphate biphasic interfacial coordination reaction to synthesize the NF membrane active layer [10]. The coating reaction was performed by reacting iron acetylacetonate in the organic phase and phytic acid in the aqueous phase. The resultant coating layer had a thickness of 13.4nm with an excellent flux of 190 $Lm^{-2}h^{-1}$ with >99% rejection towards the tested dye solution. The surface hydrophilicity is enhanced by the insertion of phosphate groups. Also, the resultant membranes showed long-term reliability, acid resistance, and antifouling nature. Zhang et al. developed modified polyamide-based NF membranes comprised of sulfonate groups [11]. The sulfonate groups were introduced by grafting 4-amino benzene sulfonic acid using carbodiimide for the crosslinking reaction. The resultant membranes showed high tolerance towards the gypsum scaling, which resulted in low scaling of the RO membrane in the subsequent process. Yin et al. fabricated a composite polyamide-based NF membrane by incorporating zwitterionic titanium dioxide (Z-TiO_2) into the top active layer via the in-situ sol-gel method [12]. The high compatibility of Z-TiO_2 with the polyamide over polyether sulfone UF support resulted in the highest water flux of 283.5 L/m^2hMPa. The optimal membrane showed >92% rejection towards Na_2SO_4 and an improved flux recovery ratio of >92%.

Though, the polyamide (PA)-based TFC NF membranes are one of the most promising and commercially available membranes for such an application. However, currently, TFC-NF membranes are not well established; for example, the PA membranes are hydrophobic and prone to fouling. Thus, this study includes the synthesis of ethylenediamine-modified multiwalled carbon nanotubes (EDA-MWCNT) incorporated thin film nanocomposite membranes prepared by our earlier reported trimesic acid (TMA) molecular self-assembly approach. TMA-based NF membranes are highly negatively charged and selective toward ionic separation compared to PA-based membranes. The synthesis of TMA-based NF membranes is facile and does not include using of the unstable and self-degradable meta-phenylene diamine reagent. Most importantly, the TMA-based membranes are hydrophilic due to the presence of abundant polar -COOH groups. The synthesized membranes were examined for their potential use in the Persian Gulf seawater pretreatment application using a custom-made pilot scale NF test unit. The study included laboratory investigations to assess and verify the feasibility of the newly developed membranes and compare their efficiency with the commercially available PA-based TFC-NF membranes. This study is important since there is no available data on the application of nano-embedded TMA-based NF membranes for the pretreatment of beach well seawater as typical Persian Gulf seawater.

2. Materials and Methods

2.1. Materials

The molecular weight cut-off (MWCO) study was performed using the different molecular weights of polyethylene glycol purchased from Merck. Also, inorganic salts such as Na_2SO_4, $MgSO_4$, NaCl, and $NaHCO_3$ used for the preliminary NF performance tests were procured from Merck. Triethylamine, trimesoyl chloride, and n-Hexane used to coat the active layer of the NF membrane were procured from Sigma Aldrich Co. The polyethersulfone UF substrate membrane with an MWCO of 5000 Da was procured from Sterlitech Corporation, USA. Ethylenediamine-modified MWCNT (EDA-MWCNT) nanoparticles used as a nanofiller during the NF membrane coating were procured from Ad-Nano Technology, India. The detailed technical specifications of the EDA-MWCNT obtained from the manufacturer are presented in Table 1.

Table 1
The specifications of EDA-MWCNT.

Parameter	Value
Purity	~99%
Outer diameter	10-20 nm
Inner diameter	5-10 nm
Length	>10 µm
NH_2 ratio	2-5%
BET Surface area	110-350 m2/g
CNT content	~95-99%
Bulk density	0.14 g/cm3
Color	Black powder
Physical form	Fluffy powder

2.2. Optimized procedure for the preparation of TFC-NF membranes

The TFC-NF membranes were prepared by coating a self-assembled trimesic acid layer over the UF membrane support. For this, the UF membranes with MWCO 5,000 Da were selected as the substrate layers. TFC membrane synthesis followed our reported protocol [13], briefly, the support membrane was placed on an A4-sized glass plate and clamped after being submerged in deionized water at 50ºC for 30 minutes. The 1.0 wt% aqueous solution of freshly prepared triethylamine (TEA, 50 mL) was transferred onto the support membrane's top surface at 25 ºC. The extra TEA solution was drained by applying compressed air. Subsequently, a solution of 0.1 wt% trimesoyl chloride (TMC) in n-hexane was poured on the TEA-coated membrane at 25 ºC. The TMC solution was allowed to react for 2 min. The TEA and TMC-

coated membrane was kept in an oven at 90 ºC for 10 min to complete the hydrolysis reaction. Fig. 1 shows the reaction scheme. Finally, the membrane was washed with water and dried at room temperature. The TFN-NF membranes were prepared using the identical protocol as that of TFC membranes. However, during coating, the nanoparticles were dispersed in the organic phase since as shown in Fig. 2, uniform dispersion of EDA-MWCNT was observed in the organic TMC solution (Fig. 2b) compared to the aqueous TEA solution (Fig. 2a).

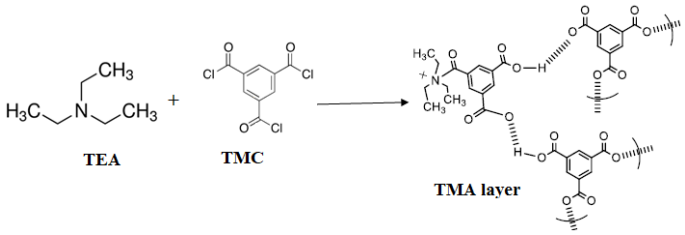

Fig. 1. The scheme of the TEA-TMC reaction to form the TMA layer.

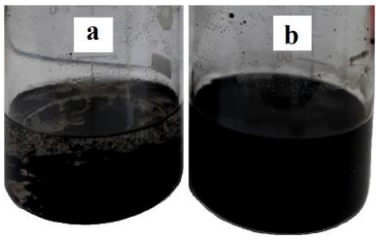

Fig. 2. Images presenting uniform dispersion of EDA-MWCNT in aqueous TEA solution (b) compared to organic TMC solution (a).

Finally, the solution of uniformly dispersed nanoparticles was coated over the PES-UF substrate using a similar protocol as discussed earlier. The different compositions of the NF membranes synthesized with their codes are presented in Table 2.

Table 2
The composition and codes of the synthesized membranes.

Membrane Code	EDA-MWCNT (Wt%)	TEA (wt%)	TMC (wt%)
M0	-	1.0	0.1
M1	0.0125	1.0	0.1
M2	0.025	1.0	0.1
M3	0.050	1.0	0.1
M4	0.10	1.0	0.1

2.3. Membrane characterization

The newly synthesized NF membranes' surface and cross-sectional morphological images were captured using a Zeiss Gemini SEM 360 scanning electron microscope instrument. A high-resolution transmission electron microscope (HRTEM) from Thermo Fisher Scientific was used to obtain the images of EDA-MWCNT. 3D-atomic force microscopic (AFM) surface images of the membranes were taken using the Nanosurf instrument, France. Utilizing contact angle measurement equipment from KINO, USA, the surface contact angles were calculated. The membrane electrokinetic potential was evaluated by measuring the streaming potential on a ZetaCAD device procured from France. Aqueous solutions of polyethylene glycol (PEG) with molecular weights Mw=100, 200, 400, 500, and 1000 Da were used to measure the MWCO of the membranes. In each experiment, the PEG feed solution concentration was held constant at 1g/L, and the rejection testing pressure was 150 psi at 25ºC. Gel permeation chromatography was used to determine the PEG concentrations in permeate samples (from GPC; Agilent Technologies).

2.4. Pre-treatment tests

2.4.1. Preliminary NF performance test procedure

The preliminary screening of the membranes in terms of flux and salt rejection was performed considering divalent salt solutions of Na_2SO_4, $MgSO_4$, and NaCl. These are the major solute constituents present in real seawater. For this, a laboratory-scale Sepa cross-flow filtration unit with an active membrane area of 20.6 cm^2 from Sterlitec Corporation, USA (product code: 1230060) was used. The filtration experiments were performed at 25–26°C and an applied pressure of 0.6 an MPa. The rejection and flux data were compared with the commercial NF-400, TS80 4040, NF-90, and NF-270 have great potential to be applied for seawater pretreatment applications.

The preliminary performance of the newly fabricated membranes was determined by maintaining similar experimental parameters. The NF filtration experiments were conducted at temperatures of 25–26 °C, at pH 7, with a flow rate of 0.8 m/s and a pressure of 0.6 MPa. In order to achieve a stable condition, the membranes were pre-filtered with DI water at 0.6 MPa before the preliminary performance tests. The NF performance of TFN-NF membranes was then tested using 1 g/L aqueous solutions of Na_2SO_4, $MgSO_4$, and NaCl. All membranes were cleaned with DI water once the tests were finished. Equation 1 was used to determine the salt rejection (R) and water flux (J).

$$J = \frac{\Delta W}{A\Delta t} \quad (1)$$

where A: effective membrane area (m^2), ΔW: the amount of water permeated (kg), J: permeate flux (kg/m^2h), and t: sampling period (h). The following equation 2 was used to evaluate the rejection coefficient R.

$$R = \frac{C_f - C_p}{C_f} \quad (2)$$

where C_f: concentrations of the feed and C_p: concentration of the permeate measured using a conductivity meter.

2.4.2. Seawater pretreatment test protocol for high-performance NF membrane

This section evaluates the real seawater pretreatment of the high-performance membrane in terms of rejection efficacy and membrane flux compared with the commercial TFC-NF membranes. The antifouling properties of the high-performance membrane are also studied. The feed water for the NF system was supplied at 26–28 °C from the beach well near the Doha west desalination plant in Kuwait. The membrane sample was compacted for an average of 60 min at 375 psi (25 bar) until the steady state flux was attained. The seawater pretreatment study was performed at a sufficiently higher pressure of 20 bar due to the higher osmotic pressure associated with the seawater. Furthermore, no chemicals were added to the NF feed as scale control acid treatment during the NF experiments. The NF test unit procured from the Convergence; the Netherlands was used for this study, and the detailed flow sheet diagram of the NF test unit is presented in Fig. 3.

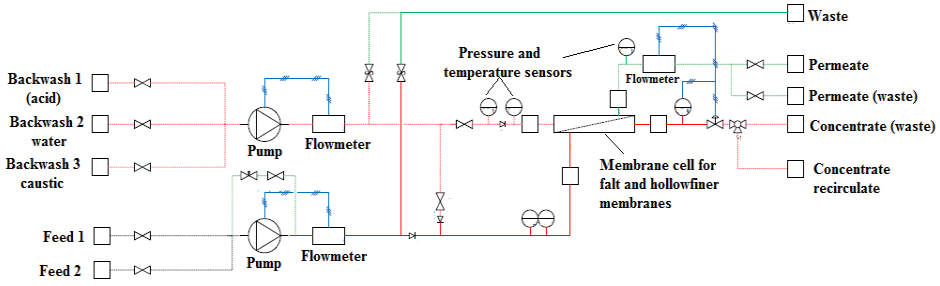

Fig. 3. The flow-sheet diagram of the NF pilot system.

2.5. The boron rejection study

The boron rejection tests for the NF membranes were executed by a methodology reported in the literature [14], wherein a 5 ppm solution of boric acid was prepared using boron standard (1000±5 g/ml) procured from Sigma Aldrich Co. Flux and rejection measurements were carried out at 25–26 °C and 0.6 MPa while the pH of the solution was changed to 6, 8, or 10 using 0.1–1 M sodium bicarbonate solutions (purchased from Merck). The concentration of boron was analyzed using inductively coupled plasma–optical emission spectrometer instrumentation from Agilent Technologies and its rejection was calculated using equation 2.

2.6. Antifouling study

The antifouling characteristics of high-performance NF membranes were evaluated using a mixture of foulant solutions. The foulant mixture consisted of $CaCl_2$ as a representative of the inorganic scaling agent and sodium alginate as natural organic matter (NOM). The composition of the foulant mixture consisted of $0.1gL^{-1}$ sodium alginate and $1.0gL^{-1}$ gypsum at 26ºC. The initial steady state flux of the newly fabricated NF membrane was attained by filtering the DI water at 0.6MPa. The foulant solution was then used in place of the feed solution, and the filtration experiment was carried out over 90 min at 0.6 M Pa to record the average flux as J_{w1}. After stopping the filtration experiment, the feed solution was changed to water that had been adjusted to pH 8.0. The membrane sample was then flushed at a high temperature of 40ºC for 30 min at 0.8MPa. Following washing, the filtration tests were carried out again using the foulant mixture at 0.6M Pa, and the average water flux was recorded as J_{w2}. The following equation 3 was used to get the relative water flux recovery ratio (FRR). The average FRR values obtained from the three repeated trials by maintaining similar experimental conditions were reported.

$$FRR(\%) = \frac{J_{w2}}{J_{w1}} \times 100 \quad \text{.....(3)}$$

3. Results and discussion

3.1. Characterization of nanoparticles and synthesized NF membranes

3.1.1. FTIR spectral study of EDA-MWCNT

The ethylenediamine-modified MWCNT procured from the manufacturer was confirmed for its chemical modification using FTIR analysis. The FTIR spectrum of EDA-MWCNT as displayed in Fig. 4 showed a peak at 1665 cm^{-1} representing the scissoring vibrations of the primary -NH_2 group [15]. The N-C-C-N stretching peak of the EDTA molecule was shown at 1507 cm^{-1}. The bending vibrations of the -C-H group were observed at 1215 $cm.^{-1}$ The -C-N stretching of the primary amine was seen at 1050 cm^{-1} [15]. The vibrations corresponding to the asymmetric and symmetric stretching of the -C-H group appeared at a range of 2361 $cm.^{-1}$

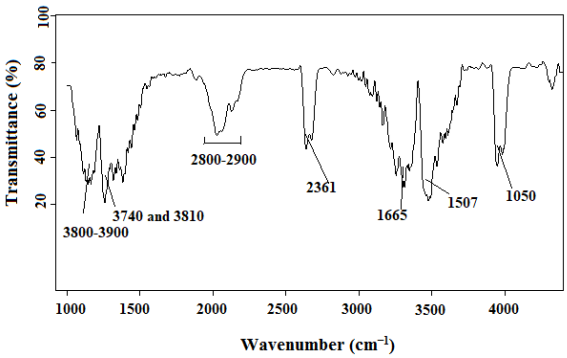

Fig. 4. FTIR spectrum of EDA-MWCNT.

Fig. 5 displays HRTEM images of EDA-MWCNT. The average outer and inner diameters of the EDA-MWCNT were 10–20 nm and 5–10 nm respectively.

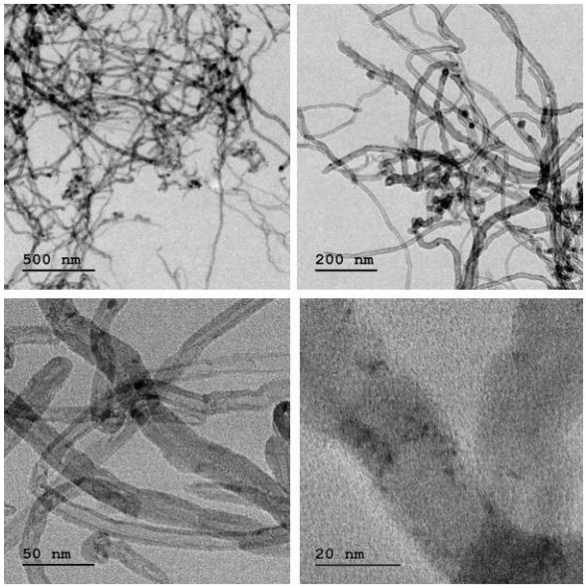

Fig. 5. High-resolution transmission electron microscope (HRTEM) images of EDA-MWCNT.

3.2. Membrane characterization

The surface images of the M1 and M3 membranes (Fig. 6a and 6b) incorporated with the 0.05 wt% of EDA-MWCNT revealed the formation of the porous structures with the presence of nanoparticles on the surface. The coating has resulted in the partial penetration of the EDA-MWCNT into the sublayer, as presented in Fig. 6c. Fig. 6c also reveals the asymmetric structures of the PES UF membrane support used for the coating of the self-assembled TMA layer. The lengthy finger-like voids were observed below the dense top layer, and the UF membrane was fabricated over the fabric support to attain good mechanical strength for the membrane. The surface of the control M0 membrane (Fig. 6e) was dense compared to the surfaces of the M1 and M3 membranes and did not display porous structures. Fig. 6f shows the cross-sectional image of the M0 membrane with the average thickness of the TMA coating layer of ~3.8µm [13].

Fig. 7 shows the AFM 3D images of the EDA-MWCNT incorporated NF and control M0 membranes. For the M0 membrane, the average surface roughness was less at 350 nm compared to the EDA-MWCNT-impregnated NF membranes. As revealed in Fig. 7 and Table 3, the M1, M3, and M4 membranes displayed increased average surface roughness of 548, 654, and 860 nm, respectively. The AFM images of the M1, M3, and M4 membranes showed an increasing trend in surface roughness parameters with the higher dosing of the EDA-MWCNT into the TMA layer. The agglomeration effect of nanoparticles and the interaction of the –NH_2 groups of the EDA-MWCNT with the TMA molecules during the self-assembly reaction resulted in rougher and denser surfaces for the resultant NF membranes.

The contact angles of the control and EDA-MWCNT incorporated NF membranes are presented in Table 3. EDA-MWCNT as a nanofiller lowered the surface contact angle values more than the M0 membrane. The increased loading of EDA-MWCNT decreased the surface contact angle values, confirming the higher accumulation of EDA-MWCNT on the membrane surfaces. From Table 3, the M3 membrane with optimal loading composition of EDA-MWCNT at 0.05 wt% showed a contact angle of 54.4°. Therefore, the hydrophilic characteristics of the EDA-MWCNT owing to the presence of –NH_2 groups reduced the surface contact angle values, which are essential to improving the permeation property of the membranes [16,17].

The lower values of the MWCO values indicate the increased density of structures on the membrane surface [18]. Fig. 8 revealed the MWCO of 170 Da for the M0 membrane as the lowest MWCO recorded amongst the NF membranes prepared in this study. Notably, the control M0 membrane showed a lower MWCO than the commercial NF-90, having an MWCO of ~190 Da, and the NF-270 membrane had an MWCO value of ~320 Da [19]. The MWCO of the EDA-MWCNT incorporated M1, M2, M3, and M4 membranes, are presented in Fig. 9. The MWCO followed the increasing trend with increased loading of EDA-MWCNT into the active TMA layer. The increased MWCO was majorly contributed by the EDA-MWCNT groups, which moved to the membrane top surface during the self-assembled layer formation and provided less dense or loose structures on the membrane surface [20]. The MWCO of the M3 membrane with the optimal loading composition was 178, also lower than the commercial NF90 and NF270 membranes.

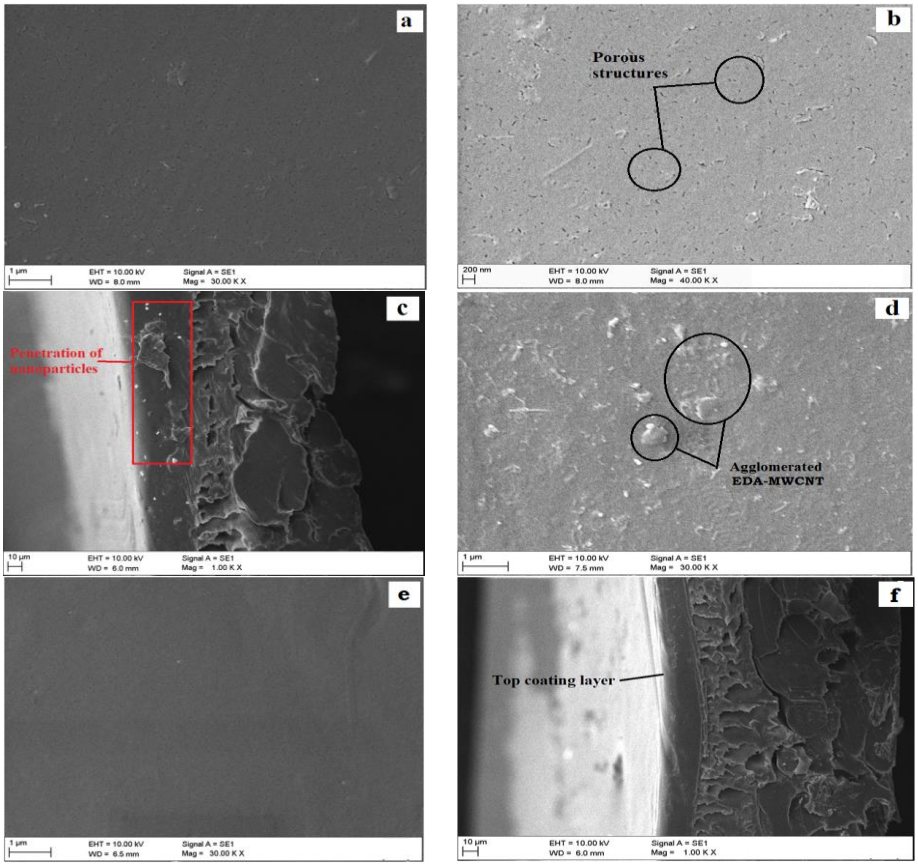

Fig. 6. SEM images of the membranes; a) surface of the M1, b, and c) surface and cross-section of the M3 membrane, d) surface of the M4 membrane, and e and f) surface and cross-sections of the M0 membrane.

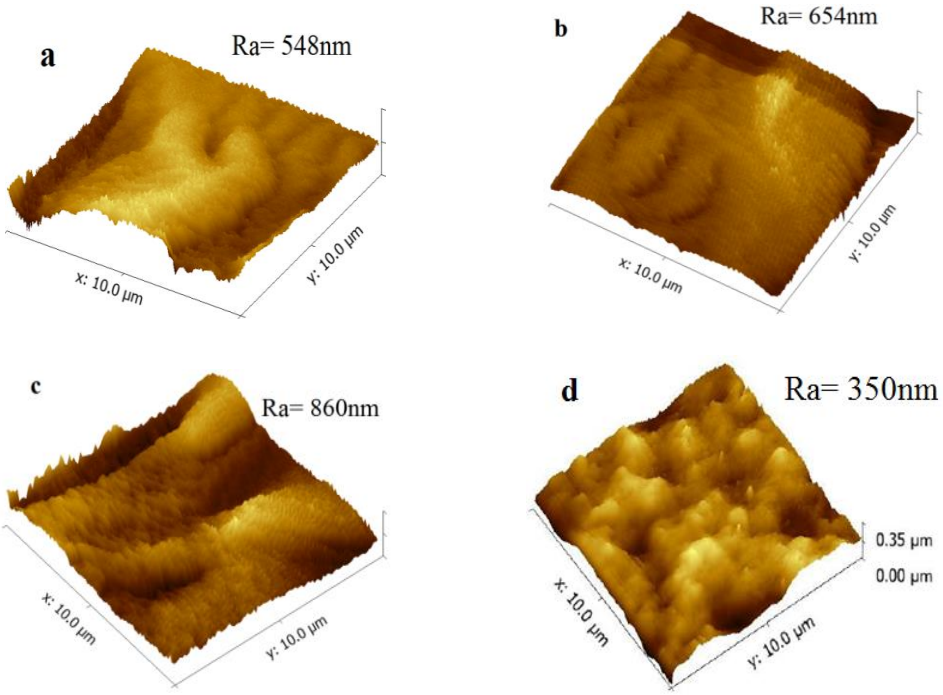

Fig. 7. Surface 3D-AFM images of a) M1, b) M3, c) M4, and d) M0 membranes.

Table 3
The contact angle and the average roughness of the synthesized NF membranes.

Membrane Code	Ra (nm)	Contact angle (°)
M0	350	56.9±0.5
M1	548	55.7±0.4
M2	595	55.0±0.7
M3	654	54.4±0.4
M4	860	53.7±0.5

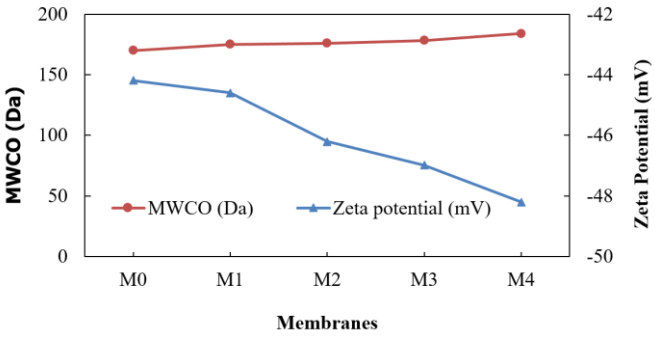

Fig. 8. MWCO and zeta potential of M0, M1, M2, M3, and M4 membranes.

As shown in Fig. 8, the M3 membrane showed a zeta potential of -47mV while the control M0 showed a value of -44.2mV. The zeta potential study revealed an increase in the negative zeta potential values at the higher dosing of the EDA-MWCNT. Thus, the EDA-MWCNT nanoparticles demonstrated their potential to enhance the negative charge on the surface of the TMA-based membranes.

3.3. Preliminary performance test results

As shown in Table 4, the rejection shown by the series of M1, M2, M3, and M4 membranes incorporated with the EDA-MWCNT nanoparticles increased with the increased loading of the nanoparticles. The rejection by EDA-MWCNT composite NF membranes was higher than the control M0 membrane. The rejection by all the synthesized NF membranes followed a similar order of Na_2SO_4>$MgSO_4$>NaCl, indicating the influence of ionic size-based sieving and charge-based Donnan effects governing the ionic separation [21]. As per the Donnan principle, the charged NF membrane surface attracts ions with opposite charges, making it easier for them to move through the membrane, while repelling ions with similar charges, aiding in keeping them in the feed solution. Therefore, the negatively charged M0 and EDA-MWCNT-based NF membrane has a high propensity to reject divalent anionic sulfate and attract divalent cationic magnesium more prominently than the monovalent chloride and sodium ions, owing to the significant interaction of the higher valency ions with the charged M0 and EDA-MWCNT-based NF membrane. Although sodium has a smaller size than magnesium, the higher rejection offered to Na_2SO_4 compared to $MgSO_4$ indicates the effect of steric hindrance between the ions and charged groups on the membrane surface. The higher rejection of $MgSO_4$ than NaCl can be explained by the sieving effect. The bigger-sized Mg^{2+} and SO_4^{2-} exhibited more rejection than the monovalent Cl^- and Na^+. The M3 corresponding to the optimal loading of the EDA-MWCNT showed the highest rejection of 97.2, 97.9, and 62.9% towards the $MgSO_4$, Na_2SO_4, and NaCl salt solutions, respectively. From Table 2, EDA-MWCNT as a nanofiller improved the permeation properties of the membranes. The optimal M3 membrane showed the highest flux of 33.6, 33.9, and 34.2 L/m^{2}h during the rejection of Na_2SO_4, $MgSO_4$, and NaCl salt solutions. Also, the M3 membrane exhibited higher flux and rejection than any commercial TS80 4040, NF-400, or NF-90 membranes.

3.4. Antifouling study results

Since fouling is primarily a membrane top surface phenomenon, the current study is essential to identify the antifouling characteristics of the TMA-coated NF membrane, a new coating technique adopted in the study.

Table 4
Performance results of newly fabricated TFC and TFN NF membranes with commercial NF membranes.

Membrane	Water flux (L/m^{2}h)			Rejection (%)		
	Na_2SO_4	$MgSO_4$	NaCl	Na_2SO_4	$MgSO_4$	NaCl
M0	29.1±0.4	28.7±0.3	29.5±0.5	98.8±0.4	97.6±0.7	60.0±0.5
M1	29.4±0.2	28.7±0.2	29.8±0.7	96.8±0.6	95.5±0.9	61.0±0.6
M2	32.2±0.6	31.9±0.5	32.6±0.6	97.1±0.1	96.3±0.6	62.2±0.1
M3	34.2±0.6	33.6±0.7	33.9±0.4	97.9±0.4	97.2±0.3	62.9±0.7
M4	33.1±0.5	32.8±0.3	32.8±0.2	97.3±0.7	96.8±0.5	62.4±0.3
TS80 4040*	31.8±0.4	33.0±0.8	33.6±0.5	97.4±0.7	97.0±0.8	40.0±0.4
NF-400*	32.8±0.8	33.6±0.6	34.2±0.3	97.0±0.4	96.8±0.3	35.0±0.8
NF 90*	18.2±0.7	17.0±0.3	14.0±0.5	98.7±0.2	98.3±0.6	59.0±0.4
NF 270*	23.0±0.6	22.0±0.5	26.0±0.5	95.1±0.8	94.0±0.5	38.0±0.7

*The commercial NF membranes were procured and tested for their preliminary rejection and flux data by maintaining similar test conditions.

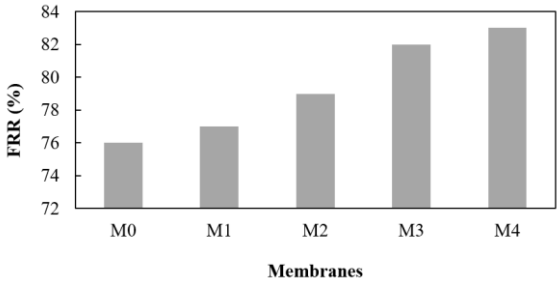

Fig. 9. The FRR values of the NF membranes.

As shown in Fig. 9, the control M0 membrane prepared by a coating of TMA layer showed an FRR of 76%, and the increasing trend of FRR after loading the EDA-MWCNT was observed. The actual contribution toward the improved antifouling property of the NF membrane was given by the diffusion of nanofillers to the TMA interface, leading to increased hydrophilicity and increased nano pathways for the transport of water molecules [22]. The higher FRR values of >80.0% are beneficial to achieving an easy cleaning of the membrane after the desalination experiment [23,24]. The improved FRR for the M3 membrane could be explained by different factors. The higher antifouling nature could be the effect of the higher hydrophilic surface attained by the M3 membrane after coating, resulting in loose binding of the foulant molecules on the membrane surface. The -OH functional groups of alginates showed a reduced propensity to attach to those NF membrane surfaces that already consist of hydrophilic -NH_2 functional groups, and the majority of the carboxylate groups of alginates were involved in bridging calcium ions [24]. Also, a weak bonding interaction was caused by the electrostatic repulsive forces between the -NH_2, functional groups present on the NF membrane surfaces, and foulant molecules [25].

3.5. Seawater pretreatment efficacy of the synthesized membranes

The flux study was performed using seawater at an applied pressure of 300 psi (20 bar) for the control M0 membrane, the high-performer M3, and the commercial NF90, TS80 4040, and NF270 membranes. The variation of water permeability of the M3 membrane incorporated with the EDA-MWCNT is presented in Fig. 10.

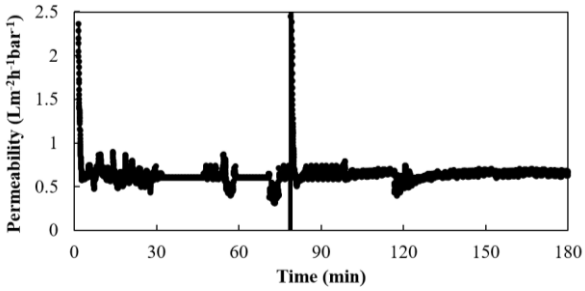

Fig. 10. Variation in permeability of M3 membrane during seawater pretreatment experiment over 180 min.

The water permeability varied in the range of 0.55–0.70 $Lm^{-2}h^{-1}bar^{-1}$ (or flux of 12.0–14.0 L/m^2h). As observed during the preliminary rejection experiments, the permeability of the M3 membrane was lower than the control M0 membrane, which could be the result of the formation of more dense structures on the M3 membrane. However, the M3 membrane witnessed a high reduction in the permeate TDS compared to the control M0 membrane, as shown in Table 5.

Table 5
Physicochemical characteristics of beach well seawater and permeates obtained from control M0, M3, and commercial NF membranes.

Parameter	Beachwell Seawater	M3	Control M0	NF-90	TS80 4040	NF-270
TDS (ppm)	34560	9635	17,700	16,800	17,400	27790
Conductivity (mS/cm)	54.44	12.3	19.36	26.25	27.34	44.39
pH	7.81	7.45	7.77	7.9	7.8	8
F^-(ppm)	4.3	0.55	0.34	3.1	3.3	3.8
Cl^-(ppm)	28631	4416	7566	12378	15890	22284
SO_4^{2-}(ppm)	3049	558	1087	27.12	25.6	36.4
Na^+(ppm)	14868	2539	3886	7463	9840	12586
Mg^{2+}(ppm)	1205	79	377	38.5	30	13.9
Ca^{2+}(ppm)	956	36	51	43.3	42	23.6
B(ppm)	4.4	1.27	1.76	3.64	3.78	3.8
Average Permeability ($Lm^{-2}h^{-1}bar^{-1}$)	-	0.5 – 0.6	0.65–0.70	0.85–0.90	0.90–0.95	2.75–2.8

For the M3 membrane, the permeate TDS was reduced to 9,635 ppm from the initial seawater TDS of 34,560 ppm during the NF experiment. The rejection offered by the M3 membrane towards the monovalent ions and boron is higher than that of the control M0 and other commercial NF membranes. Interestingly, the rejection shown by the M3 membrane towards the monovalent ionic constituents present in the seawater was much higher compared to the commercial NF-90, TS80 4040, and NF-270 membranes. The chloride and sodium concentrations were reduced to 4,416 and 2,539 ppm from their initial values of 28,631 and 14,868 ppm, respectively. This observation could be the effect of a higher negative surface charge and dense structures on the TMA-based M3 membrane, leading to a dominated Donnan principle of separation rather than a steric effect. The higher permeability and selectivity of the membrane were attributed to the combined effect of strong compatibility between EDA-MWCNT and -COOH groups of the TMA on the membrane surface [13]. Though the divalent ionic rejection of the M3 membrane was lower than the commercial NF membranes, its value was much higher compared to the neat M0 membrane. Thus, the incorporation of EDA-MWCNT into the top selective layer of the NF membrane was revealed as an efficient method to modify the NF membranes for the potential application of membranes for seawater pre-treatment applications. The denser structured M3 membrane showed >50% rejection towards the toxic boron present in the seawater at an almost neutral pH. Moreover, as shown in Fig. 11, the M3 membrane experienced a low increase in permeate conductivity over 180 min of the experimental run.

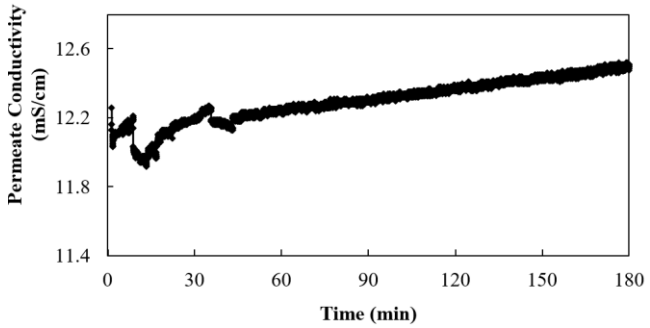

Fig. 11. Variation in permeate conductivity of M3 membrane during seawater pretreatment experiment over 180 min.

The permeate conductivity varied in the range of 12.2 to 12.4 mS/cm during the experimental run. Therefore, EDA-MWCNT as a nanofiller during the NF membrane synthesis demonstrated its high efficiency to reduce the salinity needed to apply the membrane for water-softening applications.

3.6. Boron rejection efficacy of the synthesized NF membranes

Boron is a toxic element commonly found in natural water resources like seawater and brackish groundwater. The isolation of boron is challenging using NF membrane-based technologies due to the nonexistence of a charge on boron in natural water resources. The charged NF membranes are found efficient for boron separation if they possess suitable functionalities on their surfaces to expel boron back into the feed under separation [26,27]. Therefore, in the current study, seawater boron rejection tests were conducted for all the synthesized NF membranes owing to their highly negative surface charge. The boron rejection efficacy of the neat M0 membrane in comparison with the EDA-MWCNT loaded membranes and commercial NF90 membranes are presented in Fig. 12. The M0 membrane showed high boron selectivity by displaying a rejection of ~38% at neutral pH. The possible explanation for the high boron rejection could be the repulsive interactions between the -COOH ions present on the membrane surface and the boric acid $B(OH)_3$) molecules [28]. Notably, the M0 membrane had stronger boron rejection results than the commercial NF90, which is widely used in seawater pretreatment research due to its dense top selective layer leading to high rejection [29-31]. As revealed in Fig. 12, the boron rejection offered by the EDA-MWCNT loaded membrane was higher than the neat M0 and the commercial NF membranes. The M3 membrane corresponding to the optimum performance showed a boron rejection of 42.6% at neutral pH. The increased boron rejection could be the effect of a more densely structured layer on the M3 membrane, as revealed by the MWCO study. The other observations, such as an increase in rejection with an increase in pH, are similar to the previous case studies. It was observed that the increased alkalinity (pH) of the boron solution increased the boron removal efficacy of all the membranes. It is quite obvious that the increased pH assists boric acid molecules in getting transformed into charged borate ions [32]. Thus, there is an increased repulsive interaction between the natively charged NF membranes and the borate species, resulting in increased boron rejection. At pH 11, the high-performer M3 membrane showed 95.0% rejection towards boron.

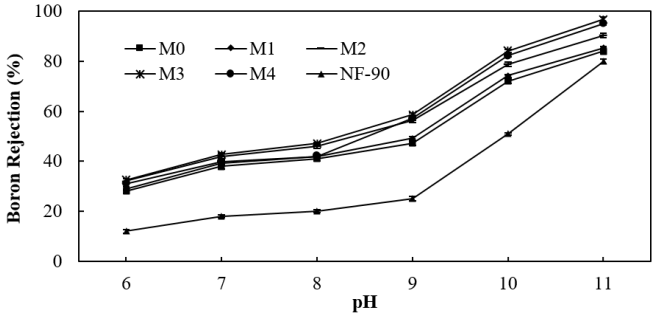

Fig. 12. pH-dependent boron rejection of the M0, M1, M2, M3, M4, and commercial NF90 membranes.

4. Conclusions

This study synthesized the aminated MWCNT incorporated TFN NF membranes for their real seawater desalination application using the Persian Gulf seawater as feed. The new membranes were highly negatively charged and denser than commercial membranes. The challenges of high selectivity with less compromise in flux loss, long-term reliability, and higher antifouling characteristics were addressed by the synthesized TFN NF membrane consisting of optimal loading compositions of the nanoparticles. The nano-based NF membranes, especially with the optimal loading composition of the nanoparticles, demonstrated better performance than four of the commercial NF membranes compared in this study. The EDA-MWCNT incorporated M3 membranes attained denser structures on their surface and showed higher stability however lower flux than control M0 and other commercial NF membranes. The membrane flux varied in the range of 12.0 to 14.0 $Lm^{-2}h.^{-1}$ The seawater TDS drastically declined in the permeate sample to 9,635 ppm from the initial seawater TDS of 34,560 ppm. The TDS reduction attained by the M3 membrane was much higher than the control M0 and other commercial NF membranes. The M3 membrane was also highly selective towards the toxic boron rejection compared to the commercial NF membranes and reduced the seawater boron concentration from 4.4 to 1.27 ppm. Again, the salt rejection shown by the M3 membrane towards the monovalent ionic constituents present in the seawater was much higher compared to the commercial NF-90, TS80 4040, and NF-270 membranes. Therefore, the new approach of NF membrane coating consisting of EDA-MWCNT as a nanofiller demonstrating its high efficiency to reduce seawater salinity will be used to apply the membrane for water softening applications.

CRediT authorship contribution statement

R. K. Alambi: Conceptualization, Roles/Writing – original draft, Supervision
M. Ahmed: Writing – review & editing, Formal analysis
G. Bhadrachari: Project administration, Methodology
M. Al- Rughaib: Data curation
J.P. Thomas: Validation; Visualization

Funding

This research received funding from the Kuwait Foundation for the Advancement of Sciences, Kuwait through grant code: PN19-15EM-05).

Declaration of Competing Interest

The authors declare that they have no known competing financial interests or personal relationships that could have appeared to influence the work reported in this paper.

Acknowledgments

The authors express their gratitude to the Director-General of Kuwait Foundation for the Advancement of Sciences, Kuwait for financially supporting this research project (grant code: PN19-15EM-05). Also, we thank the Director-General of the Kuwait Institute for Scientific Research for the continued support of the related research.

References

[1] N. Voutchkov, How can we make desalination more reliable, efficient and sustainable?, Ad. Oceanogr. & Marine Biol. 1 (2020) 4. http://dx.doi.org/10.33552/AOMB.2020.01.000520.
[2] B. Moossa, P. Trivedi, H. Saleem, S.J. Zaidi, Desalination in the GCC countries- a review, J. Clean. Prod. 357 (2022) 131717. https://doi.org/10.1016/j.jclepro.2022.131717.
[3] S. Uddin, A.N. Al Ghadban, A. Khabbaz, Localized hypersaline waters in Arabian Gulf from desalination activity—an example from south Kuwait, Environ. Monit. Assess. 181 (2011) 587–594. https://doi.org/10.1007/s10661-010-1853-1.
[4] S. Jiang, Y. Li, B.P. Ladewig, A review of reverse osmosis membrane fouling and control strategies. Sci. Total Environ. 595 (2017) 567–583. https://doi.org/10.1016/j.scitotenv.2017.03.235.
[5] C. Dong, R. He, S. Xu, H. He, H. Chen, Y.B. Zhang, T. He, Layer-by-layer (lbl) hollow fiber nanofiltration membranes for seawater treatment: Ion rejection. Desalination 534 (2022) 115793. https://doi.org/10.1016/j.desal.2022.115793.
[6] W. Zhang, X. Zhang, Effective inhibition of gypsum using an ion–ion-selective nanofiltration membrane pretreatment process for seawater desalination. J. Membr. Sci. 632 (2021) 119358. https://doi.org/10.1016/j.memsci.2021.119358.
[7] H. Alhweij, E.A.C. Emanuelsson, S. Shahid, J. Wenk, Organic matter removal and antifouling performance of sulfonated polyaniline nanofiltration (S-PANI NF) membranes. J. Environ. Chem. Eng. 10 (2022) 107906. https://doi.org/10.1016/j.jece.2022.107906.
[8] S.S. Mousavi, A. Kargari, Water recovery from reverse osmosis concentrate by commercial nanofiltration membranes: a comparative study. Desalination 528 (2022) 115619. https://doi.org/10.1016/j.desal.2022.115619.
[9] M. Zhang, X. You, K. Xiao, Z. Yin, J. Yuan, J. Zhao, C. Yang, R. Zhang, H. Wu, Z. Jiang, Modulating interfacial polymerization with phytate as aqueous-phase additive for highly-permselective nanofiltration membranes. J. Membr. Sci. 657 (2022) 120673. https://doi.org/10.1016/j.memsci.2022.120673.
[10] X. Yang, J. Huang, F. Yang, W. Wang, C. Xue, W. Zhou, Y. Wu, L. Shao, Y. Zhang, Metal-organophosphate biphasic interfacial coordination reaction synthesizing nanofiltration membranes with the ultrathin selective layer, excellent acid-resistance and antifouling performance. J. Membr. Sci. 653 (2022) 120521. https://doi.org/10.1016/j.memsci.2022.120521.
[11] W. Zhang, N. Li, X. Zhang, Surface-engineered sulfonation of ion-selective nanofiltration membrane with robust scaling resistance for seawater desalination. J. Membr. Sci. 644 (2022) 120191. https://doi.org/10.1016/j.memsci.2021.120191.
[12] Y. Yin, H. Liu, H. Li, S. Li, H. Liu, C. Wang, C. Gao, Efficient sol-gel synthesis of zwitterion functionalized titania for nanofiltration membrane with enhanced selectivity and antifouling performance. J. Taiwan Inst. Chem. Eng. 111 (2020) 252–260. https://doi.org/10.1016/j.jtice.2020.05.003.
[13] R. Kumar, M. Ahmed, S. Ok, B. Garudachari, J. Thomas, Boron selective thin film composite nanofiltration membrane fabricated via a self-assembled trimesic acid layer at a liquid–liquid interface on an ultrafiltration support. New J. Chem. 43 (2019) 3874. https://doi.org/10.1039/C8NJ05670F.
[14] Z. Ali, Y.A. Sunbul, F. Pacheco, W. Ogieglo, Y. Wang, G. Genduso, Defect-free highly selective polyamide thin-film composite membranes for desalination and boron removal. J. Membr. Sci. 578 (2019) 85–94. https://doi.org/10.1016/j.memsci.2019.02.032.
[15] L. Segal, F.V. Eggerton, Infrared spectra of ethylenediamine and the dimethylethylenediamines, Applied Spectroscopy, Sage Journals 15 (1961) 116-117. https://opg.optica.org/as/abstract.cfm?uri=as-15-4-116#articleCitations.
[16] G. Vukovic, A. Marinkovic, M. Obradovic, V. Radmilovic, M. Coli, R. Aleksi, P.S. Uskokovic, Synthesis, characterization and cytotoxicity of surface amino-functionalized water-dispersible multi-walled carbon nanotubes. Appl. Surf. Sci. 255 (2009) 8067–8075. https://doi.org/10.1016/j.apsusc.2009.05.016.
[17] J. Shen, W. Huang, L. Wu, Y. Hu; M. Ye, Study on amino-functionalized multiwalled carbon nanotubes. Mater. Sci. Eng., A, 464 (2007) 151–156. https://doi.org/10.1016/j.msea.2007.02.091.
[18] M. Safarpour, A. Khataee, V. Vatanpour, Preparation of a novel polyvinylidene fluoride (PVDF) ultrafiltration membrane modified with reduced graphene oxide/titanium dioxide (tio2) nanocomposite with enhanced hydrophilicity and antifouling properties. Ind. Eng. Chem. Res. 53 (2014) 13370–13382. https://doi.org/10.1021/ie502407g.
[19] T. Fujioka, S.J. Khan, J.A. McDonald, L.D. Nghiem, Nanofiltration of trace organic chemicals: a comparison between ceramic and polymeric membranes. Sep. Purif. Technol. 136 (2014) 258–264. https://doi.org/10.1016/j.seppur.2014.08.039.
[20] S. Dadari, M. Rahimi, S. Zinadini, Novel antibacterial and antifouling pes nanofiltration membrane incorporated with green synthesized nickel-bentonite nanoparticles for heavy metal ions removal. Chem. Eng. J. 431 (2022) 134116. https://doi.org/10.1016/j.cej.2021.134116.
[21] N. Joseph, P. Ahmadiannamini, R. Hoogenboom, I.F.J. Vankelecom, Layer-by-layer preparation of polyelectrolyte multilayer membranes for separation. Polym. Chem. 5 (2014) 1817–1831. https://doi.org/10.1039/C3PY01262J.
[22] L. Chen, X. Ren, Y. Li, D. Hu, X. Feng, W. Li, Enhancing interface compatibility of UiO-66-NH2 and polyamide by incorporating dopamine into thin film nanocomposite membranes. J. Membr. Sci. 654 (2022) 120565. https://doi.org/10.1016/j.memsci.2022.120565.
[23] V. Vatanpour, O. Karatas, S. Amiri, H.R. Rajabi, I. Koyuncu, A. Khataee, Different metal-doped ZnS quantum dots photocatalysts for enhancing the

permeability and antifouling performances of polysulfone membranes with and without UV irradiation. Chemosphere 294 (2022) 133705. https://doi.org/10.1016/j.chemosphere.2022.133705

[24] C. Balcik, B. Ozbey-Unal, B. Cifcioglu-Gozuacik, R. Keyikoglu, A. Karagunduz, A. Khataee, Fabrication of PSf nanocomposite membranes incorporated with ZnFe layered double hydroxide for separation and antifouling aspects. Sep. Purif. Technol. 285 (2022) 120354. https://doi.org/10.1016/j.seppur.2021.120354.

[25] H. Yamamura, K. Kimura, T. Okajima, H. Tokumoto, Y. Watanabe, Affinity of functional groups for membrane surfaces: implications for physically irreversible fouling. Environ. Sci. Technol. 42 (2008) 5310–5315. https://doi.org/10.1021/es800406j.

[26] Z.C. Ng, C.Y. Chong, W.J. Lau, M. Karaman, A.F. Ismail, Boron removal and antifouling properties of thin-film nanocomposite membrane incorporating PECVD-modified titanate nanotubes. J. Chem. Technol. Biotechnol. 94 (2019) 2772–2782. https://onlinelibrary.wiley.com/journal/10974660.

[27] N. Lan,; K.Y. Wang, M. Weber, C. Maletzko, T.S. Chung, Investigation of novel molecularly tunable thin-film nanocomposite nanofiltration hollow fiber membranes for boron removal. J. Membr. Sci. 620 (2021) 118887. https://doi.org/10.1016/j.memsci.2020.118887.

[28] X. Chen, W. Yuan, M. Jiang, X. Xie, Surface glycopolymer-modified functional macroporous polyHIPE obtained by ATRP for the removal of boron in water. New J. Chem. 42 (2018) 2104–2112. https://doi.org/10.1039/C7NJ03737F.

[29] B. Van der Bruggen, C. Vandecasteele, Removal of pollutants from surface water and groundwater by nanofiltration: overview of possible applications in the drinking water industry. Environ. Pollut. 122 (2003) 435–445. https://doi.org/10.1016/S0269-7491(02)00308-1.

[30] N. Hilal, H. Al-Zoubi, N.A. Darwish, A.W. Mohamma, M. Abu Arabi, A comprehensive review of nanofiltration membranes:treatment, pretreatment, modelling, and atomic force microscopy. Desalination 170 (2004) 281–308. https://doi.org/10.1016/j.desal.2004.01.007.

[31] O.A. Hamed, A.M. Hassan, K.A. Shail, M.A. Farooque, Performance analysis of a trihybrid NF/RO/MSF desalination plant. Desalin. Water Treat. 1 (2009) 215–222. http://dx.doi.org/10.5004/dwt.2009.113.

[32] Q. Zhao, D.L. Zhao, F. Feng, T.S. Chung, S.B. Chen, Thin-film nanocomposite reverse osmosis membranes incorporated with citrate-modified layered double hydroxides (LDHS) for brackish water desalination and boron removal. Desalination 527 (2022) 115583. https://doi.org/10.1016/j.desal.2022.115583.